Axial acoustic field barrier for fluidic particle manipulation

Nan Li,[1] Akshay Kale,[1] and Adrian C. Stevenson[1, a)]
Department of Chemical Engineering and Biotechnology, University of Cambridge, Philippa Fawcett Drive, Cambridge, CB3 0AS, UK

(Dated: 18 January 2019)

An acoustic field barrier integrated within a flow tubing system to achieve high-throughput separation of particles in fluid is reported in this work. We investigate the axial acoustic field of a piezo-tube with an inside diameter 34mm, length 25mm and operating frequency 1.15MHz. Energy concentrates within the tube and leakage at the ends provides a sharp monotonic acoustic pressure field within a fluidic circuit. This process is not the conventional standing wave mechanism; instead the geometry produces a spatially stable filtering action without fouling. This powerful filtering action is confirmed theoretically via a COMSOL simulation and demonstrated experimentally by concentrating suspensions of 5µm proteoglycan tracer particles at a flow rate of 20mL/min: The corresponding acoustic contrast factor is 0.243 and trapping force is 11pN. This tube geometry tackles the limitations of microfluidic standing wave based acoustic concentrators, namely complex extraction, low-throughput and distributed focus, by harnessing a stable monotonic field profile.

Keywords: acoustophoresis, acoustic, focussing, microparticle, trapping, piezoelectric, piezo

Acoustic pressure fields offer non-contact manipulation opportunities, with levitation in air receiving attention recently with stable single beam levitation[1], mid-air trapping and control[2], single axis levitation[3] and non-spherical particles in artificial field profiles[4]. Levitation of microparticles in liquids has also emerged within advanced healthcare, biotechnology research, and industrial applications such as cell culturing[5], early diagnosis of diseases[6], biomass harvesting[7] and food quality control[8].

These standing wave pressure fields have high particle concentration efficiency, rapid processing and maintenance of cell viability[9]. The primary advantage is access to physical forces that localise particles at an equilibrium point in a similar fashion as acoustic tweezers[10]. The most successful application is miniaturised lab-on-a-chip geometries[9] with standing wave patterns in submillimetre sized channels[11]. Particle separation is well controlled for half-wavelength standing wave gaps with two monotonic pressure field profiles straddling a focussing point[12].

Widening standing wave gaps to increase throughput produces polytonic regions(FIG.1.(a)) with distributed focus. This loss of focus and potential de-tune indicates standing waves in larger structures have an Achilles' heel, *i.e.* particles dont move to a single equilibrium point. Whereas living organisms sticking together via acoustic pressure waves improves harvesting[13,14] and throughput[15]. Nevertheless filtration, centrifugation, flocculation, sedimentation[16] remain attractive options.

We present a piezo-tube method to create monotonic pressure profiles with single focussing action(FIG.1.(b)). It patches the Achilles' heel of the standing wave microfludic filtration devices[17]. Here we use the piezo-tube end to pass or capture particle collectives reproducing porous filter or chromatographic medium character[18]. COMSOL simulations and tests of proteoglycan accumulation within a monotonic force field are described below.

a)Electronic mail: acs14@cam.ac.uk

The piezo-tube is excited by a radio frequency signal and generates a monotonic pressure gradient at its end. The oscillations of the electric field induce the mechanical vibrations in the wall. This energy transfers axially within the adjoining walls between the piezo-tube and adjacent elastomer coupled glass tubes and radially as an internal pressure wave. Energy along the tube walls is governed by the equations of mechanical displacement field $\mathbf{U}_S$ and the electric displacement field $\mathbf{D}_{El}$:

$$\begin{aligned} \nabla \cdot \mathbf{T}_S &= -\rho_S \omega^2 \mathbf{U}_S \\ \nabla \cdot \mathbf{D}_{El} &= 0 \end{aligned} \tag{1}$$

where ρ_S is the the mass density of the solid, ω is the angular frequency of the applied voltage and $\mathbf{T}_S$ is the mechanical stress tensor induced within the solid.

In a piezoelectric solid, $\mathbf{T}_S$ and $\mathbf{D}_{El}$ are coupled by the linear piezoelectric constitutive matrix. The stress-charge form of these relations can be expressed as:

$$\begin{bmatrix} \mathbf{T}_S \\ \mathbf{D}_{El} \end{bmatrix} = \begin{bmatrix} c_E & -e^T \\ e & \varepsilon_S \end{bmatrix} \begin{bmatrix} \nabla \mathbf{U}_S \\ -\nabla V_S \end{bmatrix} \tag{2}$$

where V_S is the electric potential field within the solid, c_E is the elasticity matrix of the material, e is the electromechanical coupling matrix of the material, and ε_S is the electric permittivity matrix of the material. While in a non-piezoelectric material of the flow tubing, the electromechanical coupling matrix e is absent, so the two energy fields can be expressed as:

$$\begin{bmatrix} \mathbf{T}_S \\ \mathbf{D}_{El} \end{bmatrix} = \begin{bmatrix} c_E & 0 \\ 0 & \varepsilon_S \end{bmatrix} \begin{bmatrix} \nabla \mathbf{U}_S \\ -\nabla V_S \end{bmatrix} \tag{3}$$

The frequency domain of the acoustic pressure field p_L in the liquid can be expressed by Helmholtz equation:

$$(\nabla^2 + k^2) p_L = 0 \tag{4}$$

where $k = \omega/c_L$ is the angular wave number, and c_L is the velocity of sound in the liquid.

The levitating pressure field in the fluid affects a particle's path: Generally the glass tubes vibrate with a weak non-uniform energy that interferes with the standing wave fields of the piezo-tube. The overall pressure field of the piezo-tube at frequencies where radial vibrations dominate over axial vibrations, leads to negligible end radiation and a sharp pressure gradient of significant force.

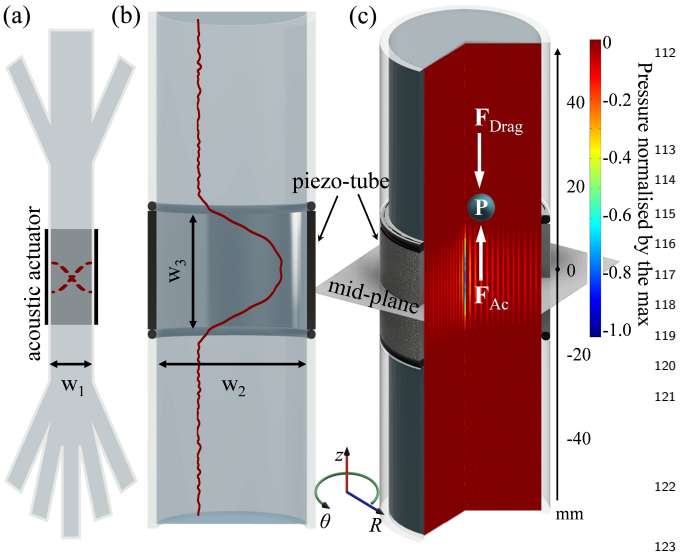

FIG. 1. The pressure gradient profiles in (a) a typical lab-on-a-chip acoustic separation setup with multiple inlets and outlets(- - -) , where w_1 is usually hundreds of microns and (b) the reported high-throughput acoustic filter(——), where w_2 and w_3 are 34mm and 25mm respectively. A COMSOL simulation of the axial acoustic pressure distribution is demonstrated on (c). The acoustic pressure field is symmetric about the mid-plane perpendicular to z-axis. It is at its strongest at z=0 and decreases along the z-axis to both the positive and negative directions until the pressure approaches a minimum value in liquid within the glass tubes. The tubing geometry is consisted in the sequence of glass tube, O-ring, piezo-tube, O-ring and glass tube.

This z-axis pressure profile is confirmed by a COMSOL simulation: In FIG.1.(c) an axisymmetric model in a cylindrical co-ordinate system is developed. Equations (1), (2), (3) and (4) are solved simultaneously. The pressure field in the liquid is driven by continuity conditions of stress and pressure at the tube inner wall. Plane wave radiation conditions are imposed at the upper and lower walls of the geometry to model energy leakage outside the piezo-tube into the flow tubing system.

The particle forces from the non-periodic monotonic gradient of its ends are determined as follows. If the diameter of the particle, d_P is smaller than the acoustic wavelength, the particle is subject to a time averaged acoustic radiation force $\mathbf{F}_{Ac}$, according to Gorkov's equation[19] as:

$$\mathbf{F}_{Ac} = -\frac{\pi}{6} {d_P}^3 (0.5 f_1 \beta_L \nabla < {p_L}^2 > -0.75 f_2 \rho_L \nabla < {v_L}^2 >) \tag{5}$$

where β_L and ρ_L are respectively the isothermal compressibility and the mass density of the liquid, v_L is the medium molecular velocity. The coefficients f_1 and f_2 can be defined as functions of the liquid and particle compressibilities and densities respectively[19,20]:

$$\begin{aligned} f_1 &= 1 - (\beta_P/\beta_L) \\ f_2 &= \frac{2[(\rho_P/\rho_L) - 1]}{2(\rho_P/\rho_L) + 1} \end{aligned} \tag{6}$$

where β_P and ρ_P respectively represent the particle compressibility and mass density

Choice of this equation is based on the necessity to calculate the force based on pressure gradients at discrete locations within the tube. This can be contrasted with conventional standing wave forces which are induced in a spatially periodic 1-D sinusoidal field. Under the influence of such a field, Equation (5) can be simplified[20] to:

$$\mathbf{F}_{Ac} = kV E_{Ac} \Phi_{Ac} \sin(2kx) \tag{7}$$

where V is the particle volume and E_{Ac} is the peak energy density dependent on the amplitude of the sinusoidal acoustic pressure field. Φ_{Ac} is the acoustic contrast factor which is a function of the densities and compressibilities of the particle and the liquid (Equation (6)). For a 1-D acoustic field the contrast factor becomes[20]:

$$\Phi_{Ac} = f_1 + 1.5 f_2 \tag{8}$$

Here, the energy density multiplied by a sinusoidal profile gives a force periodicity less than 1mm. Whereas the piezo-tube, with its non-periodic, monotonic acoustic pressure field as predicted by the COMSOL simulation, generates monotonic gradients separated by the piezo-tube length matching the form of Equation (5). This gradiant behaviour is consistent with a fraction of acoustic energy leaking out of the ends of the piezo-tube. This profile overlays the underlying radial component of the Bessel field within the fluid volume[21]. This hybrid acoustic force structure supports a particle concentration mode via the tube end geometry as the force determining variable.

The uniqueness of the present work lies in the physics of the tube-end pressure gradient for trapping particles and against a co-linear fluid flow. Whereas the remaining terms involving fluid pressure acting on the particle is based on known physics, *i.e.* the diameter of the particle d_P to the 3rd power, the energy density of the acoustic field E_{Ac} and finally the acoustic contrast factor Φ_{Ac}.

Overall transiting particles experience a significant net force field $\mathbf{F}_{Total}$, which is a vector sum of the acoustic radiation force $\mathbf{F}_{Ac}$ upwards and the Stokes' drag force $\mathbf{F}_{Drag}$ downwards due to the flow rate $\mathbf{u}_L$, *i.e.*:

$$\begin{aligned} \mathbf{F}_{Total} &= \mathbf{F}_{Ac} + \mathbf{F}_{Drag} \\ \mathbf{F}_{Drag} &= 3\pi\eta_L d_P \mathbf{u}_L \end{aligned} \tag{9}$$

where η_L is the dynamic viscosity of the liquid.

Thus particle paths resulting in concentration or leakage processes, is significantly influenced by the field $\mathbf{F}_{Total}$ which needs to exceed zero to concentrate particles. For flow rates sufficiently strong or for weak acoustic powers, $\mathbf{F}_{Drag}$ dominates over $\mathbf{F}_{Ac}$ and the particles flow along without being manipulated. As one keeps increasing the particle diameter or power, the acoustic trapping forces increase more strongly (cubic scaling) than the fluid flow-induced drag forces (linear scaling). Hence for a given acoustic wave power and a fluid flow rate, one would have a critical particle diameter below which the acoustic forces are too weak to trap particles against the drag forces.

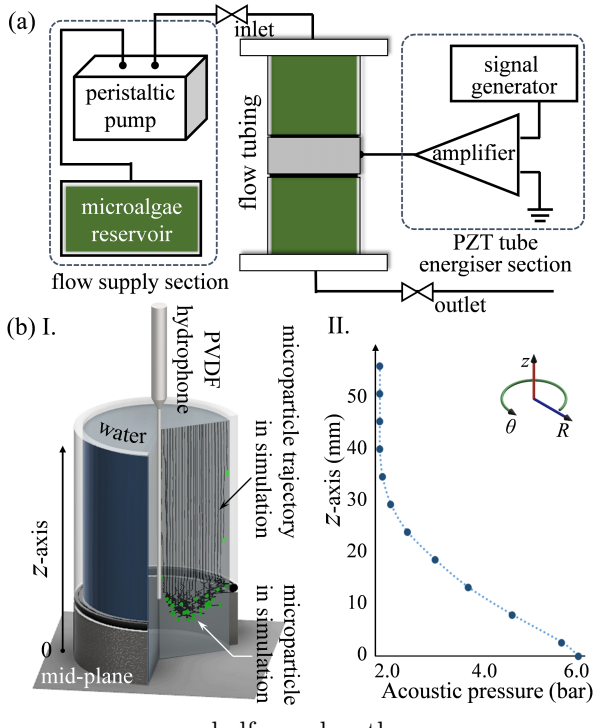

FIG. 2. (a) The high-throughput particle concentration experimental setup: Acoustic filter configuration based on a flow tubing system with passive/active tubes, piezo-tube energiser section and a flow supply system. (b) A COMSOL simulation predicts particle (•) trajectory (——) in a flow tubing system coming to a halt near the piezo-tube entrance (I). A PVDF hydrophone placed between active and passive tubes helps confirm the pressure variations of the barrier plane (II).

Also some permeability/leakage is anticipated as there are loci where the axial trapping force can vanish. These permeable regions are expected to occur along inner cylindrical planes representing the pressure nodes of the field.

TABLE I. A comparison list of density ρ_P, compressibility β_P[22], acoustic contrast factor Φ_{Ac} and the maximum acoustic force $|\mathbf{F}_{Ac}|_{max}$ of selected particles. $|\mathbf{F}_{Ac}|_{max}$ is calculated assuming the particle with a unit size, *i.e.* 1µm, in an acoustic field introduced by a piezo-tube energised with $30V_{pp}$ input at approximately 1.15MHz. $|\mathbf{F}_{Ac}|_{max}$ can be scaled as a function of the particle sizes by multiplying d_P^3.

particle	ρ_P kg/m^3	β_P Pa^{-1}	Φ_{AC}	$\lvert\mathbf{F}_{Ac}\rvert_{max}$ [a] pN
Microphyte[22]	1100	3.83×10^{-10}	0.243	0.088
WBC[23] [b]	1090	3.59×10^{-10}	0.287	0.119
Fused silica[24]	2210	1.00×10^{-11}	1.648	0.577
Polystyrene[25]	1050	2.49×10^{-10}	0.495	0.263
Gold[26]	19300	5.56×10^{-12}	2.374	0.584

[a] COMSOL predicted numbers
[b] White blood cell

Concentration or leakage is also dependent on particle contrast factors when suspended in water as shown in TABLE I. This presents the estimated traction forces in the centre of the tubular geometry according to particle type. This demonstrates dense rigid particles such as gold and fused silica are entrained by significantly higher forces, whilst biological cells have the least effect. Distinguishing from standing waves, it is important to note the axial forces are not periodic along the fluid flow direction. This results in an advantageous single concentration phase.

Particle flow rate, according to Poiseuille/laminar flow (Reynolds number for the flow rate and tube ID used in this work is 12.482), is expected to vary from the centre to the edge. At the centre it is likely to be flowing faster but also working against a stronger field (Bessel function distribution), hence there is a degree of compatibility between the flow rate and force field distribution. Overall choice of different particles of β_P, ρ_P result in different Φ_{Ac}, together with d_P lead to a variation in the $\mathbf{F}_{Ac}$. The larger the $|\mathbf{F}_{Ac}|$ is, the easier it is to manipulate the particle. TABLE. I indicates that biological cells suspended in water are the most difficult particle to capture with acoustic waves, hence for our initial experiments we have selected a biological particle; microphyte as the most challenging test for the system.

An experimental setup for demonstrating the anticipated field-particle coupling of a suspension comprising proteoglycan tracer particles (microphytes d_P of 5µm) is shown in FIG.2.(a). The flow tubing geometry consists of a piezo-tube with an OD 38mm, ID 34mm and height 25mm (APC International *Ltd.*, Type I) co-linear with two 40mm glass tubes of the same OD and ID positioned above and below. To minimise acoustic transmis-

sion an O-ring is inserted between adjoining active and passive tubes. The outer ends of the glass tubes are sandwiched between two customised acrylic sheets with liquid inlet (top) and outlet (bottom) respectively. A sinusoidal signal from the signal generator (Agilent 33120A Function/Arbitrary Waveform Generator) drives the piezo-tube at its radial mode resonant frequency and amplified by a power amplifier (EIN 310L) to approximately $30V_{pp}$. The flow of the particle suspension is driven by a peristaltic pump (Masterflex). The glass tubes allow visualisation of the particle concentration effect.

These demonstration experiments are setup to collect acoustic and optical data from the tubes via a hydrophone and camera respectively: For measuring the pressure field a PVDF hydrophone (Dr Mueller Instruments, Müller-Platte Needle Probe) was placed at the tubes axial centre (FIG.2.(b).I.) and the sampled signal amplified by a voltage amplifier (Dr Mueller Instruments, MVA 10). The result is displayed on an oscilloscope (Hantek, DSO5102P) revealing the corresponding plot shown in FIG.2.(b).II. and confirming the acoustic pressure falls significantly outside the piezo-tube.

Under the same conditions we pass the tracer particle suspension through the energised piezo-tube to get the concentration effect. Of note is the pumps flow rate, which is significantly greater than typical lab-on-chip device process by 1000 to 10000 times *i.e.* at 20mL/min. As the tube shape and depth prevent straightforward concentration measurements, the signature chromatic coordinate (Sg_{cc}) technique was chosen based on its success with assessing green foliage levels from satellite images[27,28] and the potential to profile a smaller photosynthetic system. Here the Sg_{cc} carries the RGB colour information of an image correlated with the concentration process. A 75s video is converted into an image sequence; and a consistent region of interest (ROI) is analysed frame by frame. The RGB information is recorded and the Sg_{cc} is calculated, ratioing the signature colour digit number over the sum of the red, green and blue digit numbers. The green colour is the most representative parameter, as long as the lighting levels remain fixed.

At this stage we observe a concentration effect which agrees with the form of the theoretical prediction, thus making it a suitable candidate geometry for high-throughput solid-liquid separation. A detailed COMSOL simulation also confirms the trajectory of microparticles in the flow tubing, which shows the same accumulation behaviour of the particles at the entrance of the piezo-tube as expected (FIG.2.(b).I).

Particle concentration and other motional effects were also observed: Particles influenced by the piezo-tube in either on-state or off-state is presented in FIG.3.(a). This shows the on-state creates a particle concentration effect as indicated by the relative concentrations via ROI Sg_{cc} data collected from a vertically oriented tube with downward flow. Here frames are taken of four quadrants: above and below an active tube, above and below an inactive tube (referred as on_above, on_below, off_above and off_below). Interpreting FIG.3.(b), there is a slight difference between baselines relating to small background differences in the first few frames. For the off-state as time progresses, the green and brown dashed lines indicate matching contrast above and below the tube. Whereas the on-state results in an increasing difference: The solid green line confirms that the particles accumulate above the piezo-tube, *i.e.* unable to enter the piezo-tube. Around frame 40 a minor leakage is visible, which indicates partial percolation of tracer particles through the field.

Leakage and streaming were minor relative to the trapping effect observed. For the former permeability of the field is associated with particle trajectories along the radial nodal planes, where the axial forces are weak. We hypothesise that the leakage is encouraged when the axial radiation pressure depletes along the nodal planes. As a result, we expect the leakage to be positively correlated to the number of the radial modes, although no tests were done to confirm this. However it was observed that leakage operates uniformly over the width, but is difficult to quantify due to agglomeration effects. Outside of the tube, streaming had minimal contribution to the motion of either entrant or leaked particles. From the gradient of the ROI Sg_{cc} the accumulation rate in the active tube beyond frame 70 (where the count is most accurate) is doubled, further confirming the trapping effect.

We believe this is the first demonstration of a particle trajectory arrested by an acoustic barrier derived from a large scale monotonic field. The sample flowing within this tubing system is subject to a dominant localising effect, where it concentrates at a significant volume and flow rate of 20mL/min alongside the supernatant phase. These experiments demonstrate that low contrast bioparticles can be filtered, the most challenging case, which bodes well for entities of higher contrast. A clear focal point is produced at the tube end. We no longer need to depend on the characteristics of the standing wave alone, which can become problematic at small scales and high frequencies as the particle distorts the wavefront and leads to tuning variabilities.

The membrane like filter action is the most prominent characteristic of the profile leading to an accessible accumulation which is relatively straightforward to tap. Batch type fluidic operations can immediately be applied and is amenable for series or parallel operation, with the opportunity to boost very low concentrations.

Applications include plant cell collection, animal cell purification, bioreactor systems, geological separations, agricultural processing and sensing enhancement due to the concentration factor. The approach is especially useful for particles with high acoustic contrast. Here high throughput retrofitted systems benefit from less tuning than standing wave approaches. Thus it can work within micro- or macro-liquid processing systems and support low maintenance, non-clogging and low power applications. These are powerful foundations for processing bi-

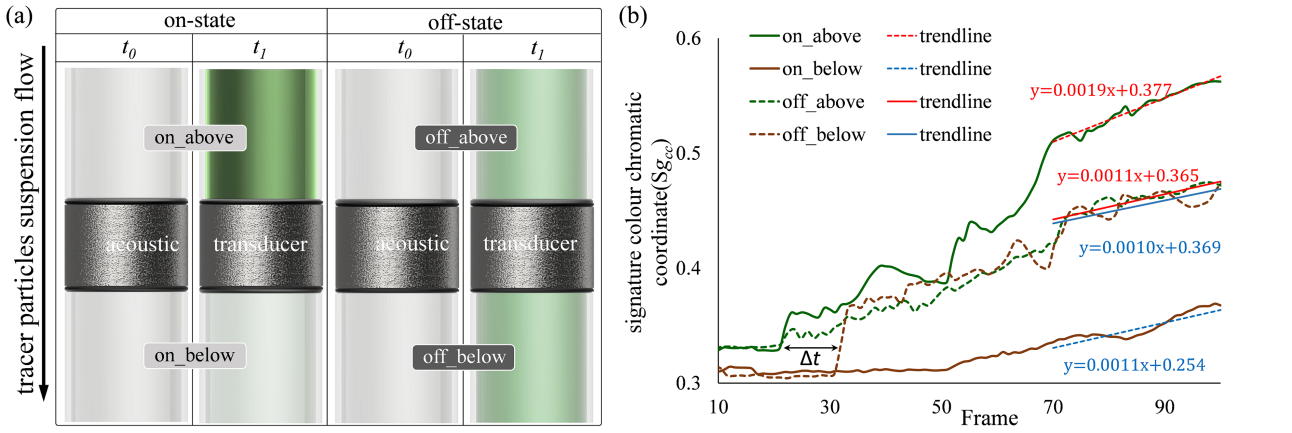

FIG. 3. Visualisation of the filtration action for a tracer particle suspension: Two sets of experiments are utilised, one with the acoustic transducer active (on-state) and the other with it idle (off-state). (a) Images taken at initial t_0 and endpoint t_1 (after 60s) show the on-state inhibits particle flow, against a fluid flow of 20mL/min. (b) Video frames capture an image sequence for dynamics of the filtration process, with relative concentration obtained from RGB digit numbers of the selected ROI. The number of frames for the tracer particle to transit the acoustic transducer is indicated by Δt. In the off-state, the marginal difference between the green and brown dashed lines indicates no particle trapping. Whereas, in the on-state, increasing differences between green and brown solid lines indicate a particle concentration effect.

ological molecules including protein and DNA and live cells where high-throughput sorting is available to meet industrial scale throughput requirements.

The authors gratefully acknowledge funding from the BBSRC (BB/NO10310/1) and Innovate UK and thank Dr Devaki Bhatta and Dr William Nock for the helpful discussions.

[1] A. Marzo, A. Ghobrial, L. Cox, M. Caleap, A. Croxford, and B. Drinkwater, Applied Physics Letters **110**, 014102 (2017).
[2] L. Cox, A. Croxford, B. Drinkwater, and A. Marzo, Applied Physics Letters **113**, 054101 (2018).
[3] T. Fushimi, T. Hill, A. Marzo, and B. Drinkwater, Applied Physics Letters **113**, 034102 (2018).
[4] H. Li, Y. Wang, M. Ke, S. Peng, F. Liu, C. Qiu, and Z. Liu, Applied Physics Letters **112**, 223501 (2018).
[5] S. Shin, D. Han, M. C. Park, J. Y. Mun, J. Choi, H. Chun, S. Kim, and J. W. Hong, Scientific reports **7**, 9907 (2017).
[6] D. M. Smalley, N. E. Sheman, K. Nelson, and D. Theodorescu, Journal of proteome research **7**, 2088 (2008).
[7] Y.-R. Hu, C. Guo, F. Wang, S.-K. Wang, F. Pan, and C.-Z. Liu, Chemical Engineering Journal **242**, 341 (2014).
[8] A. Patist and D. Bates, Innovative food science & emerging technologies **9**, 147 (2008).
[9] H. Bruus, J. Dual, J. Hawkes, M. Hill, T. Laurell, J. Nilsson, S. Radel, S. Sadhal, and M. Wiklund, Lab on a Chip **11**, 3579 (2011).
[10] X. Ding, S.-C. S. Lin, B. Kiraly, H. Yue, S. Li, I.-K. Chiang, J. Shi, S. J. Benkovic, and T. J. Huang, Proceedings of the National Academy of Sciences **109**, 11105 (2012).
[11] P. Augustsson and T. Laurell, Lab on a Chip **12**, 1742 (2012).
[12] B. Jung, K. Fisher, K. D. Ness, K. A. Rose, and R. P. Mariella Jr, Analytical chemistry **80**, 8447 (2008).
[13] F. Trampler, J. M. Piret, S. A. Sonderhoff, and D. G. Kilburn, "Acoustic filter for separating and recycling suspended particles," (1997), US Patent 5,626,767.
[14] M. D. Ward and G. Kaduchak, "Particle analyzing systems and methods using acoustic radiation pressure," (2014), US Patent 8,846,408.
[15] B. Vickroy, K. Lorenz, and W. Kelly, Biotechnology progress **23**, 194 (2007).
[16] R. G. Harrison, P. Todd, S. R. Rudge, and D. P. Petrides, *Bioseparations science and engineering* (Topics in Chemical Engineering, 2015).
[17] P. Dow, K. Kotz, S. Gruszka, J. Holder, and J. Fiering, Lab on a Chip **18**, 923 (2018).
[18] T. Imasaka, Analusis **26**, 53 (1998).
[19] H. Bruus, Lab Chip **12**, 1014 (2012).
[20] C. Reyes, L. Fu, P. P. A. Suthanthiraraj, C. E. Owens, W. Shields IV, G. P. Lopez, P. Charbonneau, and B. J. Wiley, Part. Part. Syst. Charact. **35**, 1700470 (2018).
[21] J. Yang, H. Hwang, Y. M. Bae, M. Kim, and K. Ha, Japanese Journal of Applied Physics **52**, 07HE14 (2013).
[22] E. H. Gómez, J. Tryner, A. J. Aligata, J. C. Quinn, and A. J. Marchese, Algal research **31**, 77 (2018).
[23] M. Wu, Y. Ouyang, Z. Wang, R. Zhang, P.-H. Huang, C. Chen, H. Li, P. Li, D. Quinn, M. Dao, s. Suresh, Y. Sadovsky, and T. Jun Huang, PNAS **1709210114** (2017).
[24] G. Destgeer, J. Ho Jung, J. Park, H. Ahmed, K. Park, R. Ahmad, and H. Jin Sung, RSC Adv **7**, 22524 (2017).
[25] P. Barkholt Muller, R. Barnkob, M. Jakob Herring Jensen, and H. Bruus, Lab Chip **12**, 4617 (2012).
[26] P. Kelly, *Properties of Materials* (CRC Press, 2014).
[27] A. D. Richardson, B. H. Braswell, D. Y. Hollinger, J. P. Jenkins, and S. V. Ollinger, Ecological Applications **19**, 1417 (2009).
[28] O. Sonnentag, K. Hufkens, C. Teshera-Sterne, A. M. Young, M. Friedl, B. H. Braswell, T. Milliman, J. OKeefe, and A. D. Richardson, Agricultural and Forest Meteorology **152**, 159 (2012).
[29] R. D. Perlack, *Biomass as feedstock for a bioenergy and bioproducts industry: the technical feasibility of a billion-ton annual supply* (Oak Ridge National Laboratory, 2005).
[30] P. Li, Z. Mao, Z. Peng, L. Zhou, Y. Chen, P.-H. Huang, C. I. Truica, J. J. Drabick, W. S. El-Deiry, M. Dao, *et al.*, Proceedings of the National Academy of Sciences **112**, 4970 (2015).
[31] R. Guldiken, M. C. Jo, N. D. Gallant, U. Demirci, and J. Zhe, Sensors **12**, 905 (2012).
[32] L. A. Ostrovsky, A. Priev, V. Ponomarev, and Y. Barenholz, in *Proceedings of Meetings on Acoustics 162ASA*, Vol. 14 (ASA, 2011) p. 020002.
[33] P. Collas and M. Barmatz, The Journal of the Acoustical Society of America **81**, 1327 (1987).